Faculty of Physics and Astronomy

Ruprecht-Karls-University Heidelberg

Bachelor's thesis

in Physics

written by

Ludwig Rauch

from Munich

Heidelberg, 2011

Detection of ^{133}Xe in the upper troposphere over Germany released by the nuclear power plant Fukushima Daiichi

This bachelor's thesis was written by Ludwig Rauch

and executed at the

Max-Planck-Institut for Nuclear Physics

under the supervision of

Prof. Manfred Lindner

Abstract

Detection of ^{133}Xe in the upper troposphere over Germany released by the nuclear power plant Fukushima Daiichi

After various nuclear meltdowns of the power plant Fukushima Daiichi in Japan in March 2011, large amounts of radioactive gases were released and distributed in the atmosphere. This work shows that at various altitudes and areas over Germany an increased concentration of the radioactive isotope ^{133}Xe could be measured.

This is done by a proceeding extraction of the few containing ^{133}Xe atoms from small air samples with a highly sensitive gas chromatograph. Following this, a low background measurement of ^{133}Xe β-decays with miniaturized proportional counters is done. The evaluation of the initial activity within the air samples is calculated by using the Maximum-Likelihood-Method. In the end a forward trajectory simulation developed by the DLR (Deutsches Zentrum für Luft und Raumfahrt) could be confirmed.

Nachweis von ausgetretenem ^{133}Xe aus dem Kernkraftwerk Fukushima Daiichi in der oberen Troposphäre in Deutschland

Nach mehreren Kernschmelzen im Kernkrafterwerk Fukuschima Daiichi in Japan im März 2011 konnte viel radioaktives Gas entweichen und sich somit in der Atmosphäre verteilen. In dieser Arbeit wurde gezeigt, dass in verschiedenen Höhen und Gebieten über Deutschland eine erhöhte Konzentration des radioaktiven Isotopes ^{133}Xe gemessen werden konnte.

Dies wurde erreicht, indem zunächst die wenigen enthaltenen ^{133}Xe Atome aus kleinen Luftproben durch einen hoch sensitiven Gaschromatographen extrahiert wurden. Anschliessend konnte der ^{133}Xe β-Zerfall mithilfe von miniaturisierten Proportionalitätszählrohren durch eine Messung bei sehr niedrigem Untergrund nachgewiesen werden. Die anfängliche Aktivität wurde über die Maximum-Likelihood-Methode bestimmt. Letztendlich konnte eine Vorwärts-Trajektorien-Simulation, entwickelt am Deutschen Zentrum für Luft- und Raumfahrt, bestätigt werden.

Contents

List of Figures

List of Tables

Chapter 1

Introduction

One of the strongest earthquakes in Japanese history occured at the east coast of Honshu on the 11^{th} of March 2011 and was followed by a very destructive tsunami minutes after the earthquake. This triggered a series of accidents in the nearby nuclear power plant Fukushima Daiichi which ended in the release of large amounts of radioactive gas into the atmosphere. This work confirmes the presence of ^{133}Xe in various altitudes over Germany due to a global atmospherical distribution.

1.1 The radioactive isotope ^{133}Xe

^{133}Xe is mainly produced by either neutron capture of ^{132}Xe or by fission in a nuclear power plant. Energy is gained through nuclear fission of ^{235}U, triggered by a neutron induced fission of uranium. The products are neutrons, various fission fragments and a release of energy in the order of 202.5 MeV (source: [Kay95]). In general the neutrons are used for further nuclear fissions and the energy heats up water to run a turbine. The important fission fragments for ^{133}Xe production are:

$$^{235}_{92}\mathrm{U} +^{1}_{0}\mathrm{n} \rightarrow ^{133}_{52}\mathrm{Te} +^{101}_{40}\mathrm{Zr} + 2^{1}_{0}\mathrm{n} \tag{1.1}$$

These products are unstable and will decay further.^{133}Xe is produced by the decay of tellurium:

$$^{133}_{52}\mathrm{Te} \xrightarrow[12.5\ \mathrm{min}]{\beta^-} ^{133}_{53}\mathrm{I} \xrightarrow[20.8\ \mathrm{h}]{\beta^-} ^{133}_{54}\mathrm{Xe} \xrightarrow[5.243\ \mathrm{d}]{\beta^-} ^{133}_{55}\mathrm{Cs} \tag{1.2}$$

The radioactive half life of ^{133}Xe is 5.243 days and it mainly decays by emitting a 80.997 keV photon and an electron with the engery of 346.4 keV (see figure: 1.1)

1.2 Release and distribution of ^{133}Xe in the atmosphere

The produced ^{133}Xe is captured in the nuclear fuel rod and would normaly decay without a release in the spent fuel pool after usage. During the accident in Fukushima, the earthquake and tsunami damaged not only the exterior wall of the reactor, but also, the fuel rod itself, probably due to the high temperatures from the knocked out cooling

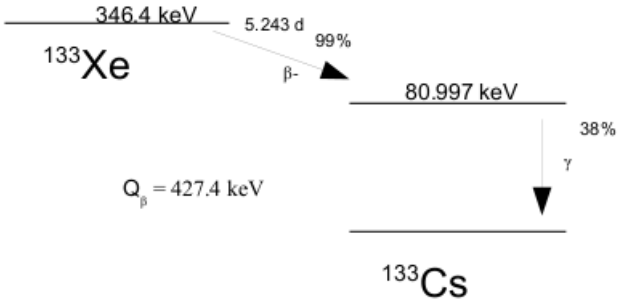

Figure 1.1: Main decay channel of ^{133}Xe. Other decay channels can be neglected due to very low possibilities (source: [Fir99]).

systems (source: [Wal11]). Thus, high amounts of radioactive gases were released into the atmosphere and were distributed over the globe. As ^{133}Xe is mainly produced during nuclear fission and neutron activation and because of the relatively short half life of 5.243 days, it is reasonable to assume that a detection of ^{133}Xe in the atmosphere is the result of a previous release by a nuclear power plant. In addition, as xenon is a noble gas, it is inert and rarely reacts with other elements. For these reasons, xenon is an excellent tracer to verify global circulation models, especially for forward trajectory calculations[1] from Japan to Germany, as the ^{133}Xe transport time is similar to its half life.

A simulation based on forward trajectory calculations can be seen in figure 1.2, which illustrates the dilution of the ^{133}Xe released in Fukushima. It was assumed that the gas release happened continuously over a couple of days, but following the latest information, this is wrong. Nevertheless, it is possible to see that the ^{133}Xe was distributed eastwards over the globe and thus, some of the radioactive gas should have arrived in Germany. A more detailed simulation for the ^{133}Xe activity in Germany can be seen in figure 1.3, which shows the vertical activity distribution versus the time for an assumed total release of $1 \cdot 10^{19}$ Bq of ^{133}Xe. Noticeable is the time delay of the xenon clouds at different altitudes. Thus, the gas arrived at high altitudes first (21.03.2011), and after three days (24.03.2011) it spread close to the surface. This can be explained by strong winds at high altitudes (jet streams) which distributed the gas very rapidly. In addition, another climatic phenomenon intensified the gas distribution. So called warm conveyor belts are able to transport large air masses rapidly into high altitudes and thus accelerated the gas spreading. The characteristics of a warm conveyor belt are not yet completely understood and the developed simulation by the DLR (Deutsches Zentrum für Luft und Raumfahrt) tries to reproduce this atmospheric phenomenon. Further information can be found in a soon to be published paper [DLR11].

The DLR started these simualtions just after the first accidents in Fukushima and thus, it was possible to predict the arrival of the ^{133}Xe plume over Germany. As the error

[1] A forward trajectory calculation is based on a simulation which contains a specific global circulation model. The DLR (Deutsches Zentrum für Luft- und Raumfahrt) developed a simulation that calculates the trajectories of released ^{133}Xe particles from Japan to Germany

of these forward trajectory calculations was unknown, the first flight was delayed until the 23.03.2011, to be sure that some gas has already arrived even though the maximum of the plume would be missed. Figure 1.4 shows the various positions of the air collections during the first flight on the 23.03.2011. Marked are the altitude and date of the various collected air samples. The airplane was equipped with a mass spectrometer to detect the anthropogenic emission products of SO_2 (green graph) and HNO_3 (red graph). The ratio of SO_2 to nitrogen oxides specifies the origin of these air accumulations, as, for instance, China uses more sulphurous coal for their power plants than Japan, this indicates air accumulations from Japan and thus potential enhanced ^{133}Xe concentrations. The black graph illustrates the flight altitude.

Table 1.1 lists the labels of various collected samples, the collection date, altitude and the corresponding simulated activities.

Sample	Date of collection	Altitude [km]	Simulated activity $[\frac{\text{mBq}}{\text{m}^3}]$
DLR2	23.03.2011	8.1	320 - 1000
DLR3	23.03.2011	9.2	320 - 1000
DLR5	23.03.2011	9.2	320 - 1000
DLR6	23.03.2011	11.8	320 - 1000
ND	14.04.2011	8 - 9	32 - 100
SD	14.04.2011	8 - 9	32 - 100

Table 1.1: Collected samples by the DLR

1.3 Gas chromatography

A highly sensitive gas chromatograph was used to extract the few ^{133}Xe atoms ($\sim$100) from small collected air samples (1-10 l). The samples were pumped over various activated-carbon filters and a gas chromatography column, to seperate the containing gases and extract the ^{133}Xe. The concentration of ^{133}Xe in the air samples was too low to measure the xenon peak by a change of the thermal conductivity in the helium carrier gas. Therefore, to avoid a blind extraction, the sample was spiked with natural xenon, which was used at the same time as counting gas[2] for the proportional counters. In the end it was possible to fill the extracted ^{133}Xe, combined with the counting gas, into the proportial counters. An more detailed description of the procedure of cleaning inert gases by gas chromatography can be read in [Lin09, Sim03].

1.4 Description of the used data acquisition system

The used data acquisition (DAQ) system is located at the Low-Level-Laboratory of the Max-Planck-Institute for nuclear physics, which was built at a depth corresponding to about 15 m water equivalence. Thereby a large amount of cosmic rays is passively shielded and the muon flux is reduced by a factor of 3. To further reduce the background, the

[2] The counting gas contains 90% xenon and 10% methane

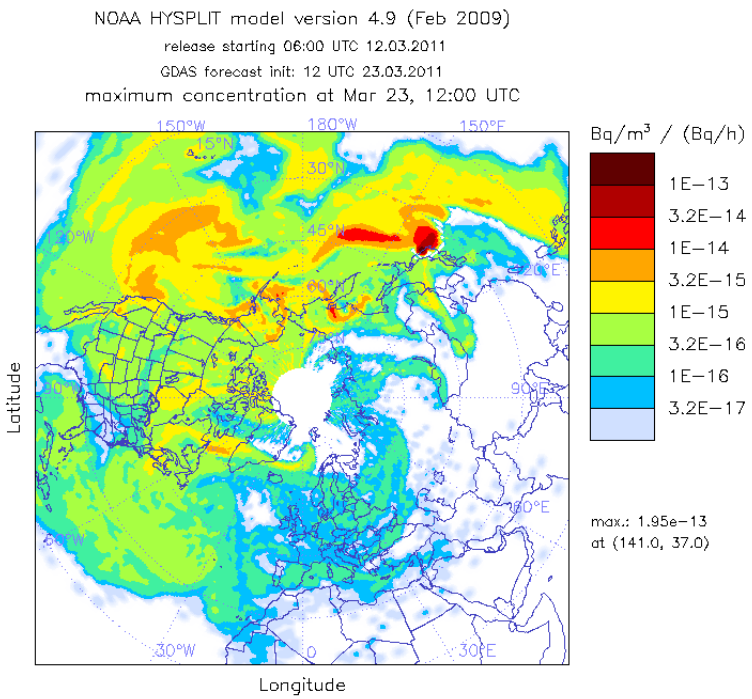

Figure 1.2: Simulation of the tropospherical ^{133}Xe dilution over the globe, based on a continuous release. The given dimensions can be interpreted as dilution. It can be seen that the source is located in Japan, as red indicates a low dilution. Afterwards the gas is distributed eastwards across the United States, the Atlantic Ocean and, finally Europe. (source: [DLR11])

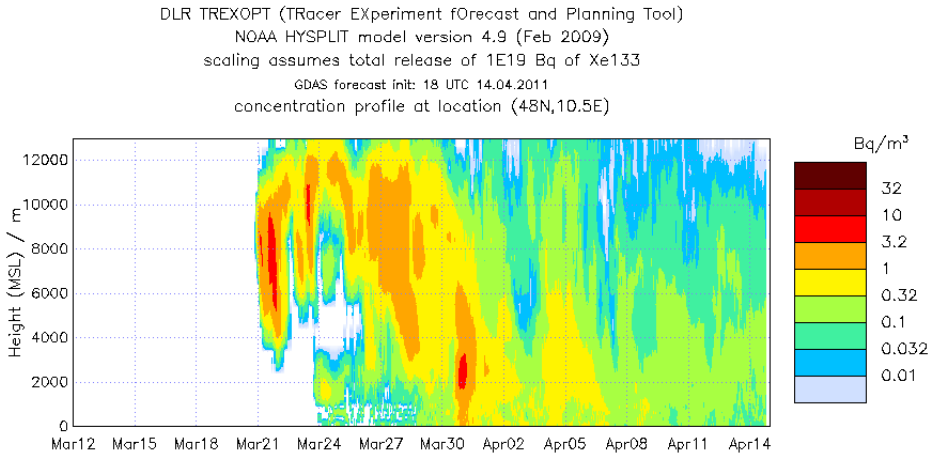

Figure 1.3: Expected vertical distribution of ^{133}Xe activity over Germany, close to the collection positions during the 12.03 and 14.04.2011, for an assumed total release of $1 \cdot 10^{19}$ Bq. This figure illustrates a first arrival of the plume on the 21.03 at high altitudes and three days after a spreading towards the ground. After a couple of days the concentration decreases due to the dilution and decay of ^{133}Xe. (source: [DLR11])

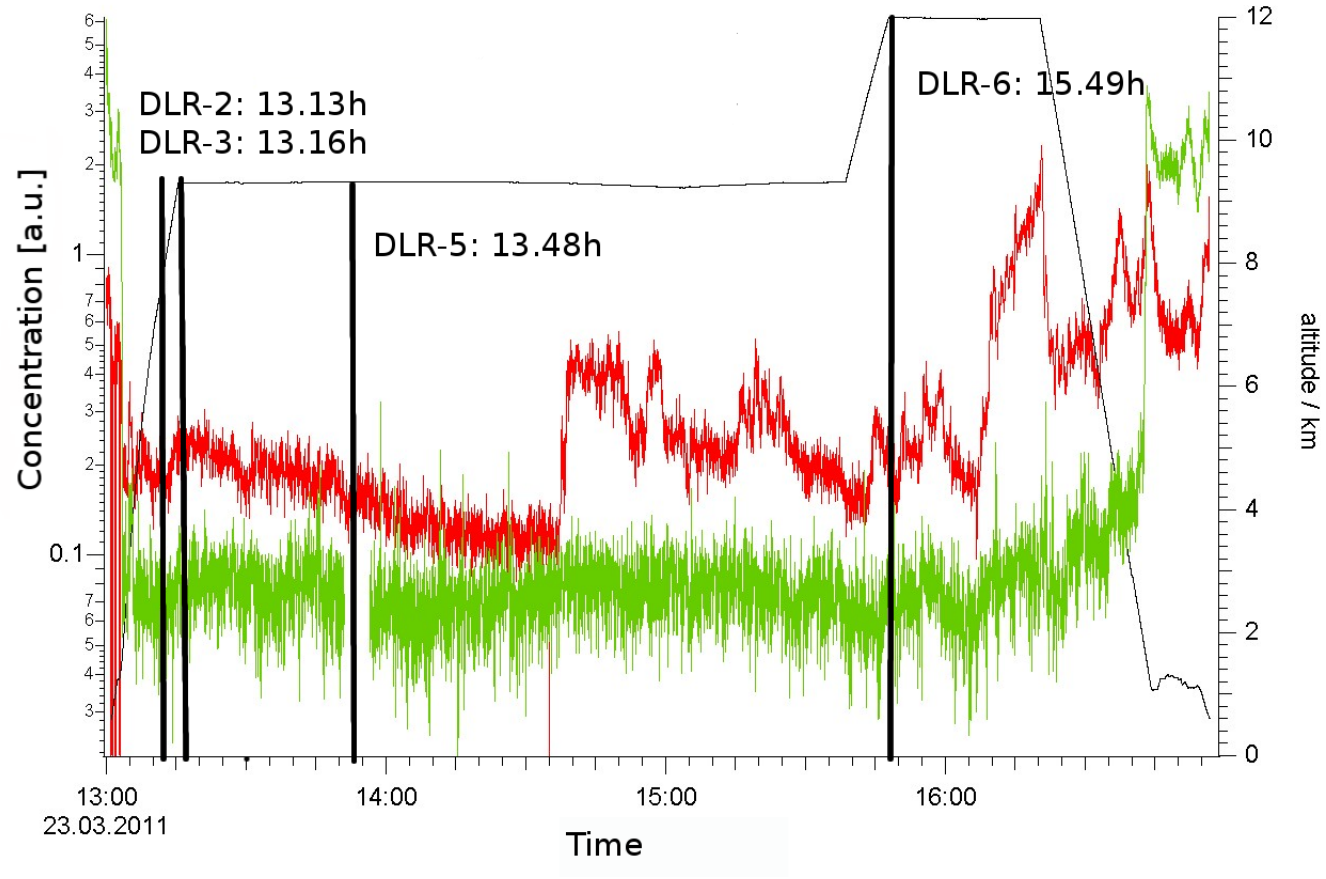

Figure 1.4: This plot shows the concentration of SO_2 (green) and HNO_3 (red) versus the time. In addition, the flight altitude (black) and the positions of the collected air samples are plotted. It was tried to use the concentration of SO_2 and HNO_3 as indicators for air masses from Japan, and therefore for potential enhanced ^{133}Xe concentrations. For instance, Japan uses different filters and coal for their coal-fired power plants than China and so these concentrations can be an indicator for the origin of air masses. (source: [DLR11])

proportional counters were placed inside a lead shield. In addition, an active muon shield is needed, as electron events of a ^{133}Xe decay and transmitting muons across the active volume of the proportional counter can not be distinguished. Therefore, the counters are surrounded by a plastic scintillator that detects transmitting myons. A schematic figure of the installed system is shown in figure 1.5.

The idea of a anticoincidence measurement is that if a muon produces a signal in a proportional counter, another signal must have been produced in the scintillator, as it surrounds the counters with an area of almost 4π and thus most of the muon signals can be excluded from the event list. The muon veto is integrated over a digital read-out system. A sofware discriminates between a single event in a counter and two signals in the counter and scintillator within a short time interval. This time interval leads to a small loss of electron events. For an area of approximatly 0.6 m^2 perpendicular to the muon flux, muon events are measured at a rate of 100 Hz. A signal is read out by the

electronics every 10ns, which leads to a dead time (20 ms) of the detector and a loss of electron events of ca. 0.2% [Lin09]. This error can be neglected for an expected event rate of between 4 - 40 counts per day. The two signals of the proportional counter and the plastic scintillator are read out by a FADC[3] board (SIS3301) and a VME PowerPC. A detailed describtion of the hard- and software can be found in [SIS04, Kih07] and [Lin09]. Each counter signal that is not in coincidence with a scintillator signal and is above a threshold is saved in a ASCII file with the indication of energy, event time[4] and rise time[5].

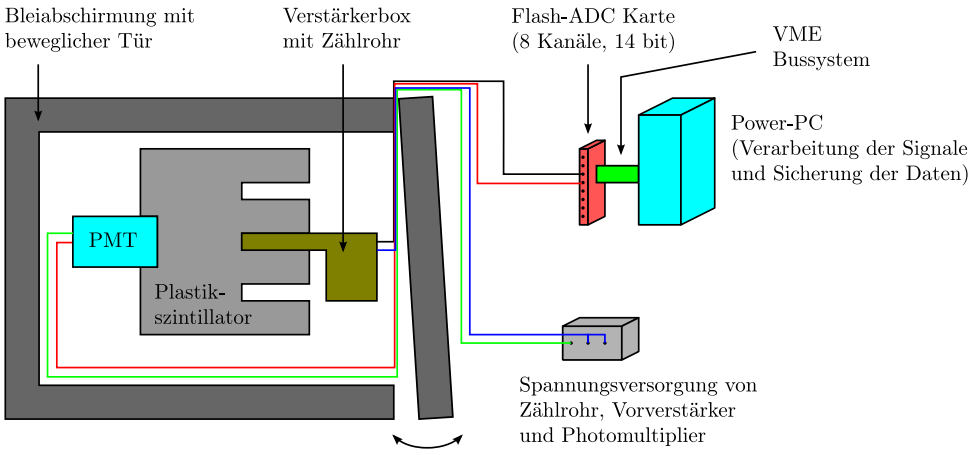

Figure 1.5: Schematic sketch of the DAQ system (source: [Lin09]).

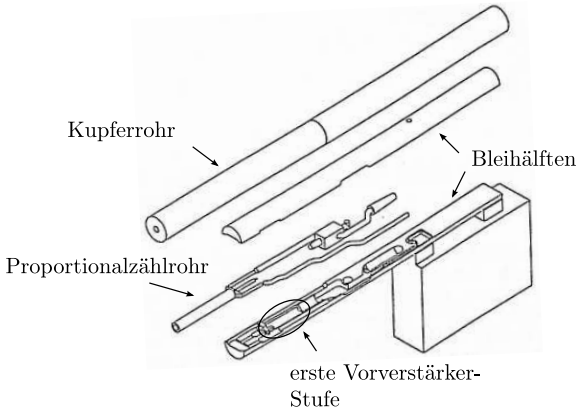

Figure 1.6: Sketch of a preamplifier and a proportional counter (source: [Heu94]).

[3] Flash - Analog to Digital converter

[4] The software is triggered by a signal from a proportional counter and saves the corresponding unix time in milliseconds

[5] The rise time is defined by the time between 10% and 90% of the signal amplitude

1.5 Miniaturized proportional counters

Highly sensitive proportional counters were developed for the Gallex project to detect the electron capture of ^{71}Ge. In this experiment they were required to measure electrons at a very low count rate, as the samples contained only a few ^{71}Ge atoms. The similar requirements[6] for a verification of low ^{133}Xe concentrations makes these proportional counters (see figure 1.7) optimal. A detailed descripton of a proportional counter can be found in [Urb89, Leo78].

1.5.1 Principle of a proportional counter

A charged particle, for instance produced from a β-decay within the active volume of a counter, various atoms of the counting gas will ionize. The applied voltage between the cathode and anode accelerates the primary positively charged ions and electrons towards the cathode/anode. The electric field around the anode is strong enough to accelerate primary electrons to ionize further atoms (secondary ionization), which allows the detection of a β-decay. Note that the mean free path of an electron with an energy of 427 keV is much larger than the diameter of these miniaturized counters and therefore it does not deposit all of its energy.

The structure of a proportional counter and one of the used preamplifier boxes can be seen in figure 1.6. To minimize the amplification of noise, a small preamplifier is located directly after the ouput of the counter. A second amplifier is used so that it can be easily detected by the FADC.

As described in figure 1.1, a 81 keV photon is emitted during a ^{133}Xe decay, which produces a signal in the scintillator. Therefore, the proportioal counter is shielded by about 5 mm of copper to absorb the photon. In the end, the amplifier box containing the counter can be placed into the scintillator, as seen in figure 1.5.

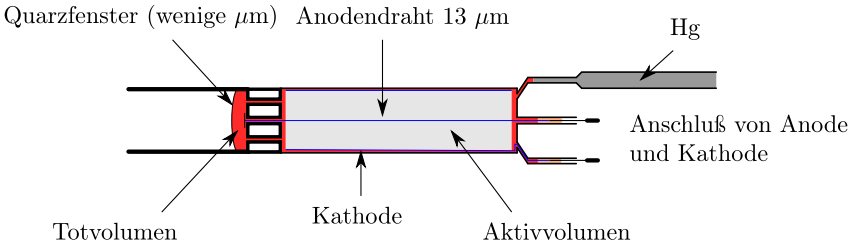

Figure 1.7: Sketch of a miniaturized proportional counter. The red color marks the dead volume (10% - 15%), the grey color the active volume (source: [Lin09])

1.5.2 Energy calibration of a proportional counter

The energy calibration in a range from 300 eV to 10 keV is done by illuminating cerium with an x-ray source. The resulting line spectrum for a 90% xenon and 10% methane based counting gas is shown in figure 1.8. This plot shows generally five different peaks,

[6] The decay energy of ^{71}Ge (233.2 keV) is similar to ^{133}Xe (427.4 keV) and thus the electron stopping power. Further information can be found in section 2.3.

which consist of a superposition of many conversion lines. A detailed description how these proportional counters are calibrated can be found in [Urb89].

Important for a calibration in an energy range between 350 eV and 35 keV are the three main peaks at 1.1 keV, 5.0 keV and 9.7 keV. Each peak consists of a superposition of various conversion lines and therefore follows the sum of many gaussian distributions. So each conversion line is described by a gaussian and all lines are summed within an accumulation of these conversion lines. The mean value is then defined by the weighted mean of the summed gaussians with respect to their intensity and is a free parameter of the fit. The 0.3 keV peak is not fitted, because it is not always clearly resolved due to its vicinity to the threshold. Also the 35 keV peak is not fitted because it sometimes overlaps with the overflow channel.

To calculate the equivalent energy for each channel, these three accumulations are fitted by a linear and a quadratic function:

Linear Fit:

$$f(E) = m \cdot E + c \tag{1.3}$$

Quadratic Fit:

$$f(E) = E^2 \cdot a_2 + E \cdot a_1 + a_0 \tag{1.4}$$

As seen in figure 1.10, the fits describe the data well for low energies (300 eV up to 10 keV) and diverge more and more for higher energies. So, the error is larger for the energy to channel allocation close to the overflow channel. The difference between the linear and quadratic fit can be used to get an estimation on this error. This could be improved if the proportional counters were driven by a lower bias voltage. This would avoid an overlap between the overflow channel and the 35 keV peak and would allow a fit for the 35 keV peak. On the other hand, the detection efficiency would be lowered for electrons from ^{133}Xe decays because a bigger fraction of the low energy electrons would not pass the detector threshold. As the energy to channel allocation is not important for the calculation of the initial activity,the focus was on the electron detection efficiency.

The counters had to be calibrated after each filling, because the pressure and gas mixture within the counters changed and thus also the mean free path of the primary electrons. Further information can be found in [Lin09].

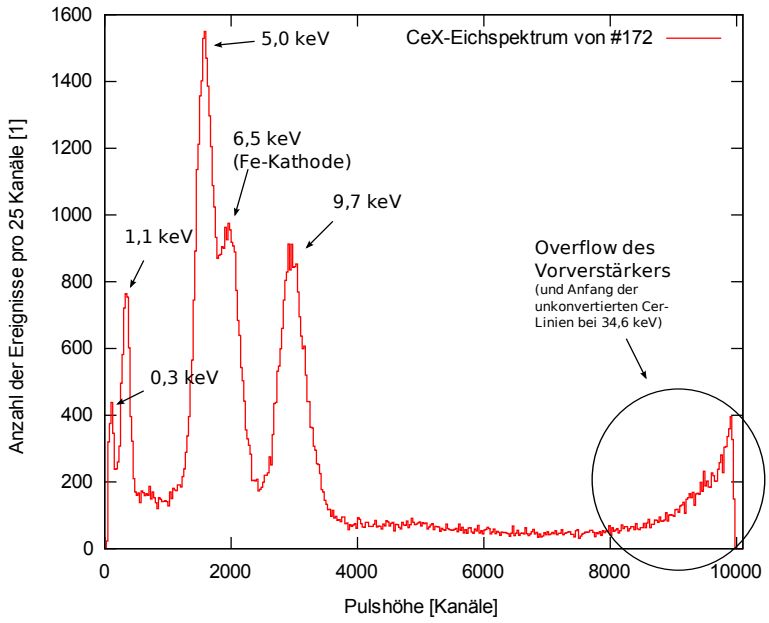

Figure 1.8: This plot shows the number of events with respect to the channels, for a cerium X-ray spectrum. The counting gas contains 90% xenon and 10% methane. Apart from the peaks at 0.3 keV, 1.1 keV, 5.0 keV and 9.7 keV, another peak at 6.5 keV can be seen due to an Fe-cathode. At channels above 9000, the superposition of the overflow channel and unconverted cerium lines (35 keV peak) is marked by a circle. [Lin09]

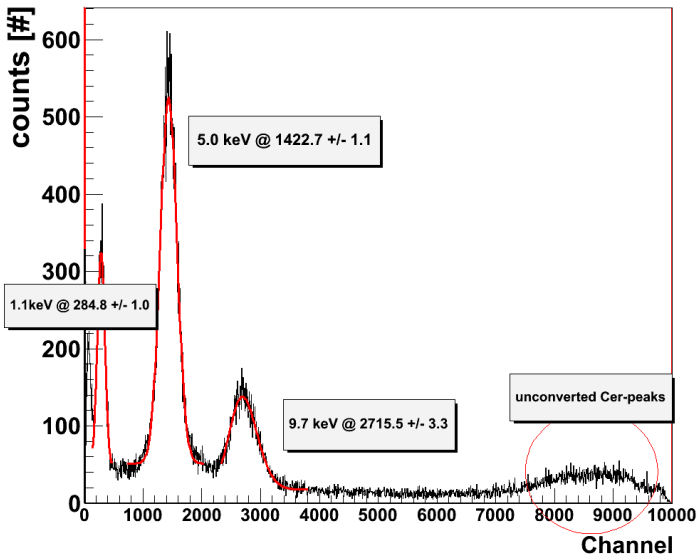

Figure 1.9: Example of a fit to calibrate the proportional counters. The red curves indicate the quadratic fit of the 1.1 keV, 5.0 keV and 9.7 keV peak. Above channel 8000 the unconverted cerium peaks overlap with the overflow channel.

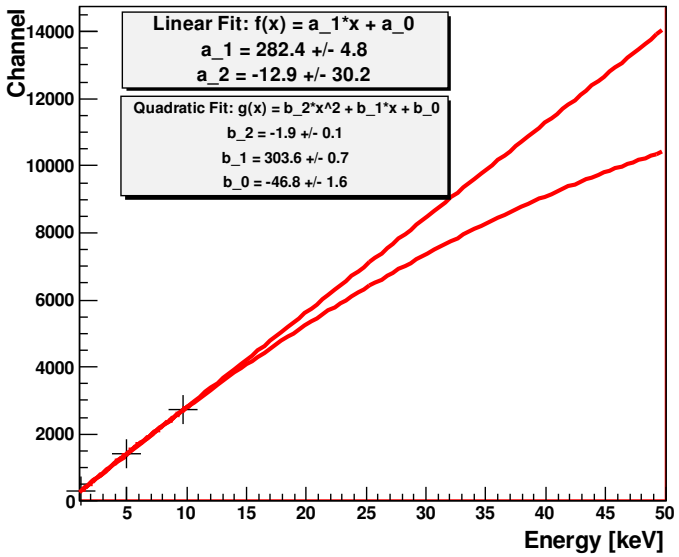

Figure 1.10: Example of a linear and quadratic fit to evaluate the energy to channel allocation. It can be seen, that the goodness of the fits is high for low energies and low for high energies.

1.6 Maximum-Likelihood-Method

Due to the high dilution of the released ^{133}Xe in the atmosphere and the small volumes of the air samples, the contained activities were very low. That maked the evaluation of the measured data difficult, as the statistic was too low for fitting the binned data to the exponential-decay law. In the following, the method of a Maximum-Likelihood analysis will be introduced briefly. For further details read [Kae07, Cle83].

1.6.1 The Maximum-Likelihood-Method

The Maximum-Likelihood-Method is a procedure that estimates unknown variables for given parameters. For example, the Maximum-Likelihood-Method estimates the number of initial atoms for given event times with a certain number of decays. Therefore, the probability has to be calculated for a given event in a hypothetical, random experiment, with respect to its defining parameters. With n beeing the number of independently measured events x_i and $\rho(x)$ a given probability density, then the probability p_α (α is the desired output parameter) is evaluated by:

$$p_\alpha = \rho_\alpha(x_1)dx \cdot \rho_\alpha(x_2)dx \ldots \rho_\alpha(x_n)dx = \prod_{i=1}^{n} \rho_\alpha(x_i)dx \tag{1.5}$$

This allows a definition of the Likelihood function $\mathcal{L}$:

$$\mathcal{L}(\alpha) = \prod_{i=1}^{n} \rho_\alpha(x_i) \tag{1.6}$$

Note that the function $\mathcal{L}(\alpha)$ is not a probability distribution, as α is not a random variable.

The estimated value $\hat{\alpha}$ is then defined as the value that maximizes the function $\mathcal{L}(\alpha)$. For a numerical determination of $\hat{\alpha}$, it is easier to write the equation (1.6) as:

$$-\ln \mathcal{L}(\alpha) = -\sum_{i=1}^{n} \rho_\alpha(x_i) \tag{1.7}$$

The equivalence of equation (1.6) and (1.7) is given by the strictly monotonic behaviour of the logarithm function. The calculation is done with the numerical minimization program MINUIT (source: [Jam98]). Because of the change of the sign, equation (1.7) has to be minimized.

1.6.2 Error calculation

The distribution around the maximum $\hat{\alpha}$ of the likelihood function $\mathcal{L}(\alpha)$ is generally not symmetric but, in the limit $\mathrm{n} \to \infty$, a gaussian distribution around $\hat{\alpha}$ can be approximated (source: [BL98]).

$$\mathcal{L}(\alpha) \approx \mathcal{L}(\hat{\alpha}) \exp\left(-\frac{1}{2\sigma^2}(\alpha - \hat{\alpha})^2\right) \tag{1.8}$$

This can be written as a logarithm function with respect to the error σ of the estimated value.

$$\ln \mathcal{L}(\hat{\alpha} \pm k\sigma) \approx \ln \mathcal{L}(\hat{\alpha}) - \frac{1}{2}k^2 \tag{1.9}$$

The estimation of the error σ of the estimated value $\hat{\alpha}$ is done by the variation of α, in order to reduce equation (1.7) by a factor of 2. For more than one free parameter $\alpha, \mathrm{b}, \mathrm{c}$ the error is calculated by the minimization of $\mathcal{L}(\hat{\alpha} \pm \sigma_\alpha, \mathrm{b}, \mathrm{c})$ with respect to b and c, whereas σ_α is varied until the difference is $\frac{1}{2}$.

$$\ln \mathcal{L}(\hat{\alpha}, \hat{\mathrm{b}}, \hat{\mathrm{c}}) - \ln \mathcal{L}(\hat{\alpha} \pm \sigma_\alpha, \mathrm{b}, \mathrm{c}) = \frac{1}{2} \tag{1.10}$$

1.6.3 The Likelihood function

To evaluate the data, two free parameters are needed. One for the background rate b, which is approximatly constant in time, and one for the number N of initial ^{133}Xe atoms. The half life is a fixed parameter, since the statistic is too low. The derivation of this particular likelihood function can be found in [Kae07].

Generally two different probabilities have be taken into account. On the one hand, the probability for the various events at times t_i has to be calculated and on the other

hand, the probabilty for no decay between two events. Multiplying these probabilities gives:

$$p_{\mathrm{N,b}} = \prod_{i=1}^{n} p(1, t_i, t_i + dt) \cdot \prod_{i=1}^{n} p(0, t_i, t_{i+1}) \tag{1.11}$$

This leads to:

$$-\ln \mathcal{L}(\mathrm{N}, \mathrm{b}) = \int_{t_0}^{T} \left(\frac{\mathrm{N}}{\tau} e^{-t/\tau} + \mathrm{b} \right) dt - \sum_{i=1}^{n} \ln \left(\frac{\mathrm{N}}{\tau} e^{-t_i/\tau} + \mathrm{b} \right) \tag{1.12}$$

With t beeing the time, T the time period of a measurement, $\tau = 5.243$ d the half-time of ^{133}Xe, N the number of initial ^{133}Xe atoms and b the background rate. For practical reasons, the measurement was interrupted several times, which lead to various measured time intervals $[t_{a_k}, t_{e_k}]$. To combine all intervals, all measurements k were simply added together

$$-\ln \mathcal{L}(\mathrm{N}, \mathrm{b}) = \sum_{k} \int_{t_{a_k}}^{t_{e_k}} \left(\frac{\mathrm{N}}{\tau} e^{-t/\tau} + \mathrm{b} \right) dt - \sum_{i=1}^{n} \ln \left(\frac{\mathrm{N}}{\tau} e^{-t_i/\tau} + \mathrm{b} \right) \tag{1.13}$$

In the end the, equation (1.13) has to be minimized in order to evaluate the number of initial atoms and the background rate.

Chapter 2

Evaluation

2.1 Collected and measured air samples

As described in the introduction, the first flight and collection of the air samples was done by the DLR just 12 days after the nuclear desaster in Fukushima Daiichi. These samples arrived at the Max-Plack-Insitut for nuclear physics soon after the collection and it was possible to start the measurements on the 28.03.2011. A second flight was done on the 14.04.2011 and the measurements began on the 23.04.2011. The labels of the collected air samples, their volume at 1013 hPa and the total measured time can be found in table 2.1. This table shows the small sample size. It was not possible to collect more air at such short notice due to the limited air container sizes and official regulations.

The following sections explain the error analysis for these measurements. First of all, the loss of ^{133}Xe has to be taken into account due to the extraction procedure. Afterwards, the detection efficiency of the counters for ^{133}Xe and the cut efficiencies have to be evaluated in order to correct the results of the Maximum-Likelihood fit. In addition, it was necessary to correct the number of initial atoms due to a ^{222}Rn contamination, which could be quantified through the signature of ^{214}Bi and ^{214}Po decays.

Sample	Volume at 1013 hPa [l]	Total measured time [d]
DLR2	0.79	72.2
DLR3	0.79	60.1
DLR5	0.79	65.3
DLR6	0.79	44.2
ND	9.96	31.6
SD	9.75	31.6

Table 2.1: Measured samples collected by the DLR

2.2 Loss of ^{133}Xe due to the extraction procedure

As described in section 1.3, the ^{133}Xe atoms were extracted by a gas chromatograph. In practice it is not possible to seperate and extract 100% of a gas. This would lead to a systematic underestimation of the initial ^{133}Xe concentration, if it stayed unconsidered. Several reasons can explain the loss of ^{133}Xe. The biggest loss of xenon[1] can be attributed to the chromatography procedure, as some of the xenon breaks through the adsorber column too early or the tail of the release peak must be cut in order to avoid an ^{222}Rn contamination. In addition, some of the xenon will be adsorbed within the traps. A volume measurement of the used xenon before and after each mixing with the air samples quantifies the loss of xenon and thus the loss of ^{133}Xe. Another error can not be avoided, as it is impossible to fill all xenon into the counters. This residual gas can be measured and considered in the analysis, which is usually negligible compared to the other losses. The calculated total loss of ^{133}Xe is shown in table 2.2.

Probe	Loss[%]
DLR2	5.3
DLR3	15.2
DLR6	8.3
DLR5	7.8
ND	6.9
SD	9.8

Table 2.2: Evaluated loss of ^{133}Xe due to the extraction procedure

2.3 ^{133}Xe detection efficiency

To evaluate the data, it is essential to know the detection efficiency for ^{133}Xe in each of the used proportional counters. It can be assumed that the detection efficiency for ^{133}Xe is similar to ^{85}Kr, because the decay energy[2] is in the same order of magnitude and therefore the energy deposition within the active volume of a counter. The electron stopping power in xenon for various electron energies is plotted in figure 2.1. It can be seen that the stopping power is very similar for the two given decay energies and, as both decays show similar beta spectrum, it can be reasonably assumed that the efficiencies will be in the same range. Soon it will even be possible to directly measure the ^{133}Xe efficiency, as a ^{133}Xe standard will be delivered from the United States.

The detection efficiency for ^{85}Kr and the acceptances for the over- and underflow cuts have been already determined ([Lin09]) and until the measurement with a ^{133}Xe standard is performed, an efficiency of $(65 \pm 5)\%$ is assumed[3].

[1] Here it is necessary to distinguish between the ^{133}Xe from the air samples and the used xenon as counting gas. During the extraction procedure, the air containers which contain the ^{133}Xe, are first spiked with a certain amount of natural xenon and then the xenon mixed with the ^{133}Xe is seperated by

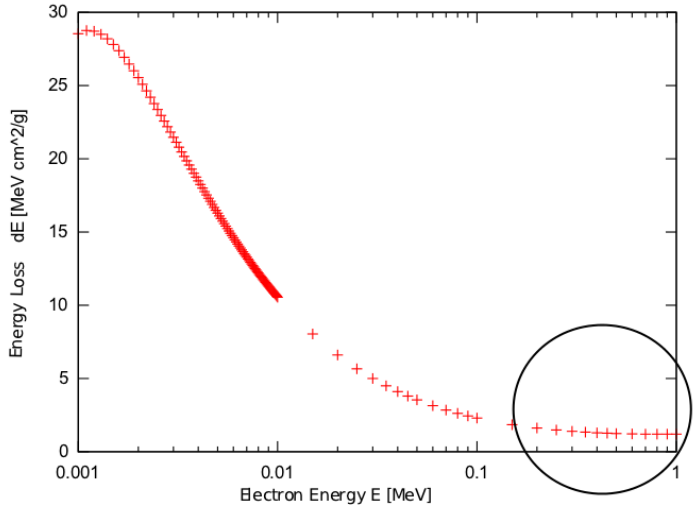

Figure 2.1: In this plot, the electron stopping power in xenon is plotted versus the electron energy. The circle marks the electron energy range of ^{85}Kr and ^{133}Xe. In this range the slope is very low and therefore the difference of the stopping powers is small. (source: [Lin09, NIS09])

2.4 Cut acceptances

To exclude events from the evaluation that are not triggered by a ^{133}Xe β-decay, it is necessary to set up cut conditions. These unwanted events can be triggered by noise from the read out system, by undetected muons[4] or by a ^{222}Rn contamination (see section 2.5) of the samples.

2.4.1 Overflow cut

Alpha particles, for instance produced in the uranium series (see table 4.2), are very likely to trigger an event in the overflow channel. Since the mean free path in the counting gas is shorter for alpha particles than for electrons, they deposit more energy in the counter. This can be seen in figure 2.2 which shows an energy spectrum of a ^{222}Rn standard. The events above 35 keV are mainly triggered by alpha particles, produced by the decay of ^{222}Rn and therefore, have to be excluded from the analysis. The cut acceptance correction for the overflow cut is included in the approximation for the ^{133}Xe detection efficiency described in section 2.3.

gas chromatography from the other gases to fill the proportional counters.

[2] 427.4 keV (^{133}Xe) and 687 keV (^{85}Kr)

[3] This assumption is based on an error of 4% for the detection efficiency (source: [Kae03]) and 1% for the different stopping powers

[4] It is possible that a muon passes the muon Veto because the scintillator does not surround the counters completly by 4π

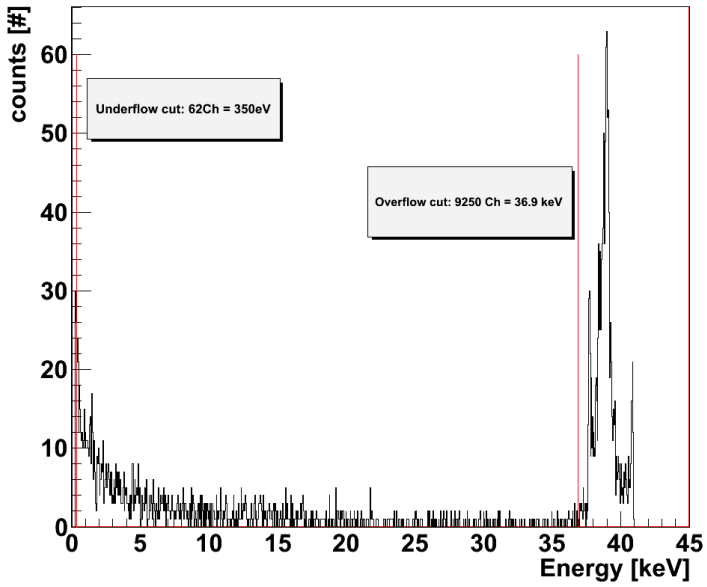

Figure 2.2: An energy spectrum of ^{222}Rn, for which the peak at the overflow channnel is mainly triggered by alpha particles and, thus, a cut at channel 9250 (36.9 keV) excludes most of the alpha events.

2.4.2 Underflow and rise time cut

The characteristics of noise events are shown in figure 2.3. One measurement of the SD sample is noticeable for its high number of events (489) in a relative short measured time period of three days. This can not be explained by a high concentration of ^{133}Xe or ^{222}Rn, because most of the events show a long rise time[5] at a low energy. These are not events triggered by an electron or alpha particle, since these would show shorter rise times. Therefore they can be distinguished from signals of ^{133}Xe β-decays by a rise time cut of 5 μs and a maximum energy of approximatly 350 eV.

The validation of this assumption can be seen in the recorded puls shapes in figure 2.4. Electrons deposit more energy than noise events. This leads, through the ionized counting gas, to a fast increase (ca. 1μs) in the measured voltage and thus, to a short rise time in the recorded pulses. The decay time is long in comparison, as it is dependent on the capacitors' discharge speed. However, it can be seen that, through a low energy to noise ratio, the low energy pulses are delayed and it is possible that they will be mistakenly cut. This error will be considered in the cut acceptances.

In conclusion, good events have to fullfill the following conditions: A rise time below 5 μs, an energy above 350 eV and an energy below approximately 35 keV (the energy equivalent to channel 9250).

A fraction of ^{133}Xe events will be lost due to these cuts and, therefore, it is necessary to quantify a cut acceptance. This can be done with the data of a cerium X-ray calibration,

[5] The rise time is defined by the time between 10% and 90% of the puls height.

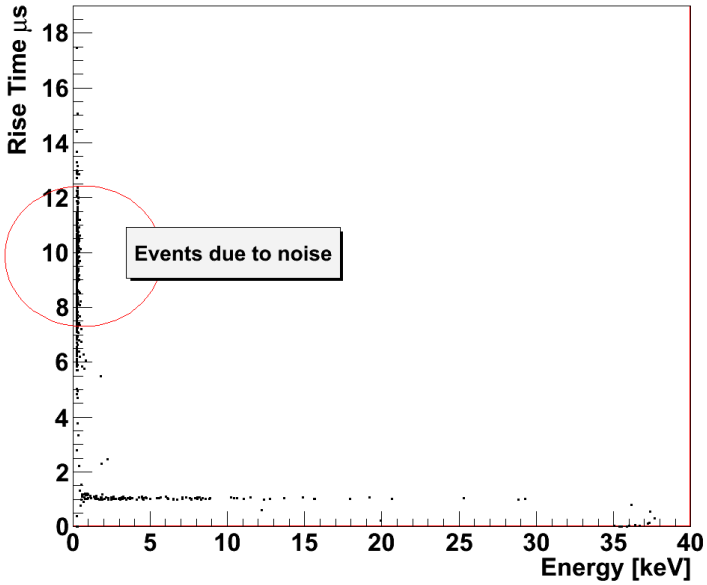

Figure 2.3: Events due to noise from the electronics are marked with a red circle. This population show rise times above 5 μs and energies below 350 eV. Most events in this population can be excluded by a rise time cut of 5 μs.

as the conversion electrons of the xenon gas indicate the expected energy range for ^{133}Xe β-decays. The energy distribution of these events can be seen in table 4.1.

In figure 2.5, the calibration data (red markers), as well as the cuts for the DLR 2 sample, is plotted. In addition, the acceptance curve (red) for the rise time cut versus the measured data is plotted. It is a priori not clear that the rise time cut acceptance can be calculated by the cerium X-ray calibration, as the X-rays generate only conversion electrons within the counters. This is different for a ^{133}Xe β-decay, which produces not only electrons, but also positively charged ions. This would make the rise times of the signals longer. However, the rise time cut is only important for low energies and as the dominant factor for the rise time delay is the low signal to noise ratio, the time difference is small. To correct the measured data (black histogram), it has to be convoluted with the rise time cut acceptance curve (red). The corrections are in the order of less than 1 % and therefore negligible.

The cut acceptance correction for the underflow cut is included in the approximation for the ^{133}Xe detection efficiency described in section 2.3. Soon it will be possible to directly measure the cut acceptances for each counter, once the measurement of a ^{133}Xe standard is performed.

Of course, it is impossible to cut all events that are not related to a ^{133}Xe decay, as some of them show the same characteristics, for example, ^{210}Pb decays or undetected muons. But it can be reasonably assumed that these events are constant in time and are therefore included in the background rate.

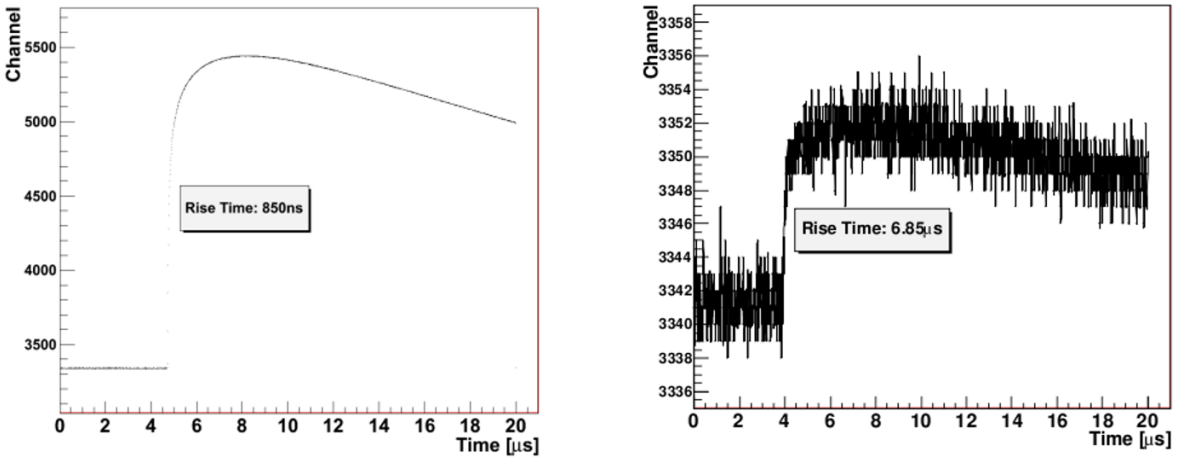

Figure 2.4: This plot shows the puls shape of a typical electron event (left) and a noisy electron event (right). The axes are the recored voltage in arbitrary units verus the time. The electron event is saved by the electronics after puls shaping with the indication of a rise time of 850 ns. The right puls shape is an example of a low energy event, which passes the threshold (channel 20) but the raise time is delayed by noise, as the signal to noise ratio is very low. This event is saved with the indication a rise time of 6.85 μs and will be mistakenly cut.

2.5 Consideration of a ^{222}Rn contamination

^{222}Rn is produced by the decay of radium ^{226}Ra (radium series) and, is, thus contained in ambient air, depending on local geological properties. It is not exactly known which concentration is present at the heights of collection. In addition, the properties of the inert gases radon and xenon are very similar, so it is very difficult to seperate xenon and radon through gas chromatography, which could easily lead to a radon contamination in the counters. As seen in table 4.2, ^{222}Rn and its daugthers decay by emitting three alpha particles and two electrons. Theoretically, a proportional counter would detect five decays for only one ^{222}Rn atom. However, a proportional counter might detect recoil alphas or through electrons produced by x-ray emissions. It is very difficult to calculate the number of ^{222}Rn events and thus, a ^{222}Rn standard has to be measured. In additon, it is not possible to distinguish between the atoms by their half lifes[6], as they are very similar and the statistics is too low to consider a ^{222}Rn decay in the Maximum-Likelihood analysis. Therefore, it is important to detect a ^{222}Rn contamination and correct the fit results, which would otherwise lead to a systematic overestimation of the initial number of ^{133}Xe atoms. For these reasons, a ^{222}Rn standard of (1.2 $\pm$ 0.1) mBq was filled into a proportional counter and measured over 5 days.

[6] 3.82 days (^{222}Rn) versus 5.243 days (^{133}Xe)

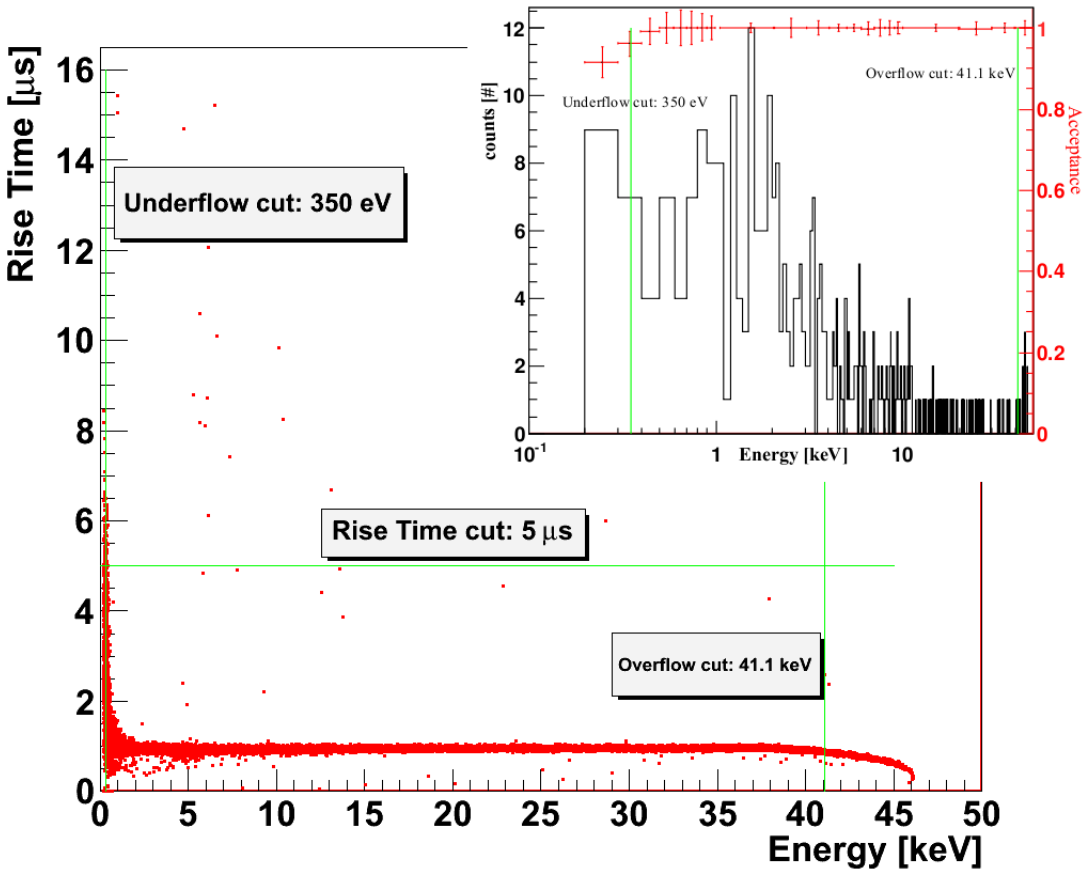

Figure 2.5: The figure illustrates the calibration data (red markers) of the DLR 2 sample with a cerium X-ray source and the green lines indicate the cuts. The acceptance curve (red) for the rise time cut and the energy spectrum (black) of the DLR 2 data can be seen in the upper right figure. The x-axis shows the logarithm of the energy and the green lines indicate the energy cuts. It can be seen that for low energies the rise time cut acceptance is below 1. However, the highest count rate for ^{133}Xe decays can be found in this energy range. Nevertheless, the result of a convolution of the measured data with the rise time cut acceptance curve corrects the data less than 1 % and can therefore be neglected.

2.5.1 BiPo detection efficiency

A so called BiPo event describes the decays of ^{214}Bi and ^{214}Po. These two decays together show a specific characteristic and can be used for a detection of ^{222}Rn. On the one hand, these two atoms decay almost coincidently since the half life of ^{214}Po is only 164.3 μs and, on the other hand, the ^{214}Po decay will likely produce an event in the overflow channel, when an alpha particle with 7.8 MeV is emitted. With the limited time resolution of the used DAQ system, it was not possible to resolve the decay sequence and, thus, the two signals of ^{214}Bi and ^{214}Po decays were identified within the same 10 ms time interval.

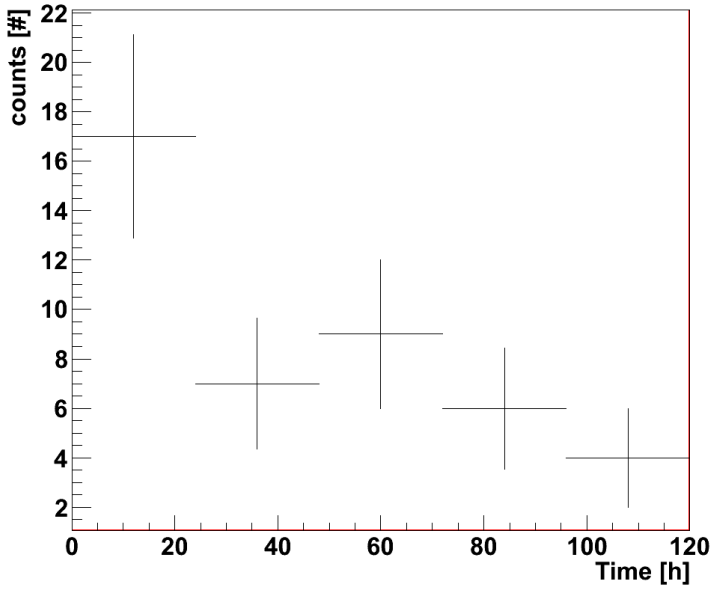

Figure 2.6: This histogram shows the counts per day versus the measured time up to 120h. It illustrates the decay of BiPo events and proves that the conditions explained in section 2.5.1 only apply for BiPo events.

This is only a problem of the used software, which is not optimized for events occuring in such short time intervals. But it is reasonable to assume that the possibility of two independent events within 10 ms is negligible, especially for the low expected count rates. With the conditions that two signals have to be in a time interval of 10 ms and one of them triggeres the overflow event, a BiPo detection efficiency of (13 ± 2)% could be determined. To prove that these conditions only apply for BiPo events, the time stamp for each BiPo signal was recorded and plotted verus the time (see figure 2.6). A decay can clearly be seen.

Through the energy spectrum of the ^{222}Rn standard, it can be determined that one BiPo event produces an average of 16 ± 5 events in an energy range between the under- and overflow channel. It is important to mention that, due to the possibility of an emitted high energy photon from a ^{214}Bi decay (see table 4.4), which is able to pass the copper shield of the counter, a BiPo event could be detected by the muon veto system.

2.5.2 Corrections due to a ^{222}Rn contamination

With the conditions for BiPo events explained in section 2.5.1, the measured data was scanned for these events and it was possible to detect 2 BiPo events in the data of the DLR 2 sample. With the calculated ratio that one BiPo event corresponds to 16 ± 5 events in the energy range between the under- and overflow channel, the DLR 2 sample had to be corrected through a reduction of the initial ^{133}Xe atoms by 32 ± 9. Since it was not possible to detect any other BiPo event in the other measured data, it is assumed

that these probes were free of ^{222}Rn.

2.6 Results from the Maximum-Likelihood-Analysis

To evaluate the data the Maximum-Likelihood approach described in section 1.6 was used. The results are shown in table 2.3. It can be seen that the fit results deviate from zero significantly.

Sample	Number of initial ^{133}Xe atoms [#]	Background [cts/day]
DLR2	67.1 ± 11.7	3.9 ± 0.3
DLR3	101.3 ± 15.1	8.1 ± 0.4
DLR5	44.6 ± 11.0	3.5 ± 0.3
DLR6	79.6 ± 13.3	1.2 ± 0.3
ND	54.7 ± 14.1	6.6 ± 0.6
SD	85.7 ± 26.1	34.5 ± 1.3

Table 2.3: Results from the Maximum-Likelihood analysis

2.7 Histograms for the measured samples

The histograms, shown in figure 2.7, illustrate the decay of ^{133}Xe over a certain period of time. Each bin represents a measured time interval of one day. It can be seen that, at the beginning of the measurement, the counters contained a certain number of ^{133}Xe atoms that decayed over time. At the end of the measured period the background rate dominated the ^{133}Xe β-decays. These plots contain a number of seperate measurements, which leads to a systematic error for the edging bins within each measured interval, because these bins do not contain data from 24 hours. The error of each bin is calculated using the square root of the total number of events within one day.

In contrast to an obvious decay in the DLR 3 sample, the data of the SD sample seems to plot a high and constant count rate. Despite that, the Maximum-Likelihood fit calculates an initial number of atoms equal to 86 ± 26, which is significantly different within 3σ to zero. The advantage of the used fit is the independence of the bin size, as every count is accounted for seperately. This prevents a loss of information of the event times, that would otherwise be caused by the splitting of the measured signals into bins. Thus, it is possible to fit a ^{133}Xe decay, even though it seems that the high background dominates.

2.8 ^{133}Xe concentration in the atmosphere

A comparison between the measured and simulated activity is only possible if all previous results are taken into account. This is done by consideration of the loss of ^{133}Xe due to the cut acceptances (see section 2.4), the ^{133}Xe detection efficiency (see section 2.3) and the loss of ^{133}Xe due to the extraction procedure (see section 2.2). Therefore, the results

of the Maximum-Likelihood analysis have to be corrected and it is possible to obtain the number of atoms per volume from the air containers collected at a pressure of 800hPa. This was converted and calculated with equation (2.1) to dimensions of becquerel per cubic meter at the time of collection. The results are shown in table 2.4.

$$\mathrm{A(t)} = -\frac{d\mathrm{N}}{dt} = \lambda \cdot \mathrm{N(t)} = \mathrm{A_0} \cdot \mathrm{e}^{-\lambda \mathrm{t}} \tag{2.1}$$

with A beeing the total activity, λ is the decay constant and N for the number of initial particles.

Table 2.4 compares the simulated and measured activities in Germany on the 23.03 and 14.04.2011. It can be seen that both values match each other within the errors. This confirmation is astonishing, since the simulation predicted the dilution of ^{133}Xe for a trajectory around half the globe correctly.

Sample	Date	Activity A $[\frac{\mathrm{mBq}}{\mathrm{m}^3}]$	Simulated activity $[\frac{\mathrm{mBq}}{\mathrm{m}^3}]$
DLR-2	23.03.2011	240 ± 103	900 - 9200
DLR-3	23.03.2011	738 ± 124	1100 - 3400
DLR-5	23.03.2011	304 ± 79	1100 - 3400
DLR-6	23.03.2011	547 ± 101	1600 - 5100
ND	14.04.2011	45 ± 12	100 - 300
SD	14.04.2011	75 ± 23	100 - 300

Table 2.4: Measured and simulated activities for the air samples collected by the DLR

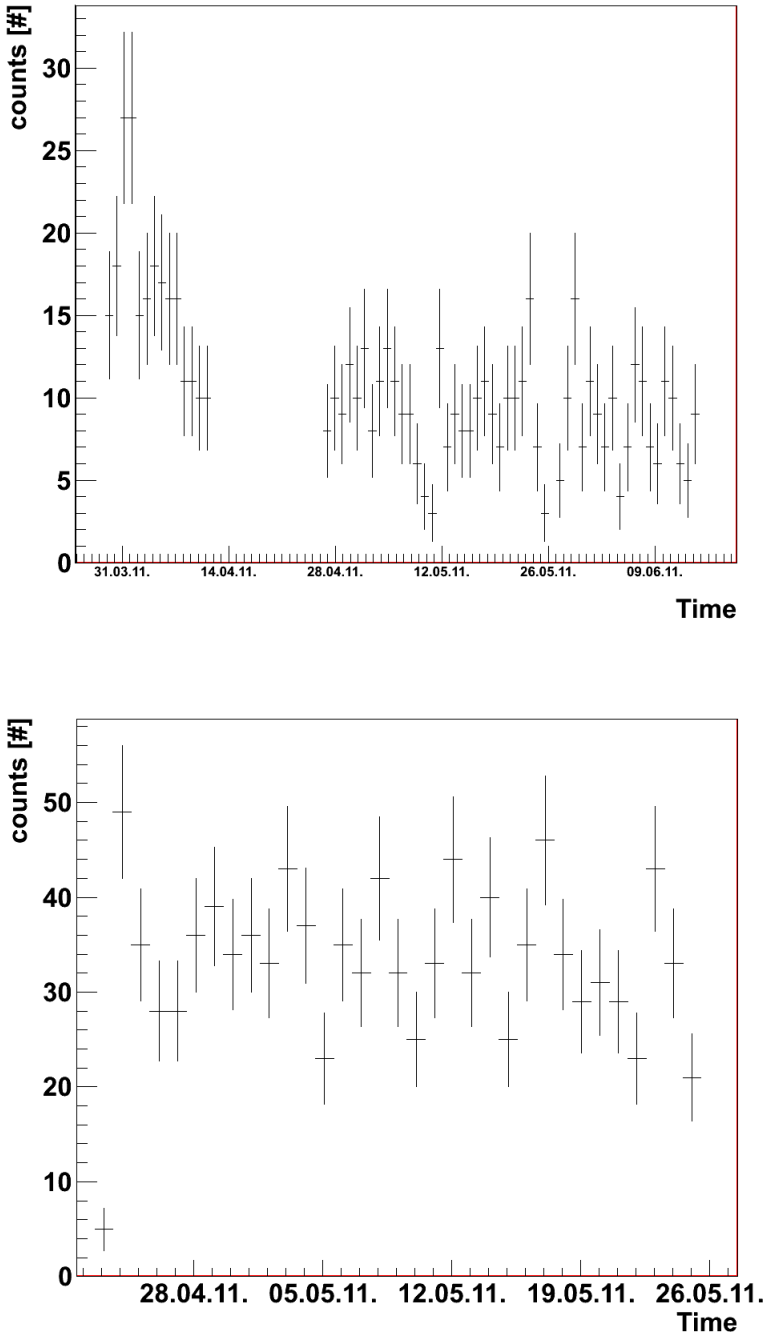

Figure 2.7: The upper histogram shows the data of the DLR 3 sample in a time period of 60 days and the lower histogram the SD sample in a time period of 32 days. The data is plotted with the cut conditions explained in 2.4 and each bin represents one day. Note that the histograms contain data from several measurements which leads to a systematic error for the edging bins, as they do not contain data from one whole day. The DLR 3 sample shows at the beginning a decay and to the end background dominates. In contrast the data of the SD sample seems to show a high and constant count rate, but with the Maximum-Likelihood-Method it is possible to calculate a number of initial atoms which deviate to zero significantly.

Chapter 3

Conclusion

This work shows that, after a release of radioactive gas from Japan, an increased concentration of ^{133}Xe in the upper troposphere over Germany could be measured. This measurement was achieved in collaboration with the DLR (Deutsches Zentrum für Luft und Raumfahrt). They were able to take air samples in the size of (1-2)l by plane, at heights of up to 10km, just twelve days after the nuclear desaster in Fukushima Daiichi.

The measurement was performed by a proceeding extraction of around 100 ^{133}Xe atoms from the 1 liter samples. Afterwards, the extracted ^{133}Xe was filled into specially designed miniaturized proportional counters for a low background measurement. This was done at the Max-Planck-Insitute for nuclear physics inside the Low-Level-Laboratory so as to reduce cosmic rays. In addition, an anticoincidence system had to be installed in order to veto transmitting muons.

The data acquisition system recored not only the event times of signals but also saved information about the rise times and deposited energies. Thus, it was possible to distinguish noise from electron events by a cut acceptance of close to 100% and it was even possible to detect a radon contamination with a BiPo detection efficiency of $(13 \pm 2)\%$.

In the end, the cut data was evaluated with the Maximum-Likelihood-Method for two free parameters, one for the number of initial ^{133}Xe atoms and for the background. The parameter for the half life of ^{133}Xe had to be fixed, as the statistics were extremly low. Out of the fit results, the corresponding activity was calculated, after corrections for the counter efficiency and losses of ^{133}Xe, due to the extraction procedure. In the end, a forward trajectory simulation that was developed at the Deutschen Zentrum für Luft und Raumfahrt could be confirmed.

Outlook Another inert tracer with a similar half life might be ^{222}Rn, which could be emitted by volcanic eruptions and transported into the upper troposhpere. However, it can be assumed that the background of ^{222}Rn is higher than ^{133}Xe, as radon is produced in the uranium series. It will be tried by the DLR to fly through clouds of volcanic emissions and collect air samples in order to detect an increased ^{222}Rn concentration. The low background measurements and highly sensitive extraction procedures used in this work will be necessary to be enable ^{222}Rn as a tracer on global scales.

Chapter 4

Appendix

4.1 K-shell X-ray lines of cerium and xenon

Linie	Cerium		Xenon	
	Energy (keV)	rel. Intensity	Energy (keV)	rel. Intesity
$K_{\alpha 2}$	34.279	54.7	29.459	54.1
$K_{\alpha 1}$	34.720	100	29.779	100
$K_{\beta 3}$	39.170	9.7	33.564	9.39
$K_{\beta 1}$	39.258	18.8	33.625	18.2
$K_{\beta 5/1}$	39.542	0.115	33.875	0.092
$K_{\beta 5/2}$	39.560	0.157	33.889	0.127
$K_{\beta 2/1}$	40.222	2.06	34.409	1.88
$K_{\beta 2/2}$	40.239	3.99	34.418	3.65
$K_{\beta 4/1,2}$	40.338	0.057	34.498	0.041
$K_{\beta 2/3,4}$	40.428	0.862	34.552	0.67
K-absorption boarder	40.443		34.561	

Table 4.1: K-shell X-ray lines of cerium and xenon

4.2 Radium series

Nuclid	Decay	Half life	Energy [MeV]	Fission Product
^{226}Ra	α	1602 a	4.871	^{222}Rn
^{222}Rn	α	3.8235d	5.590	^{218}Po
^{218}Po	α	3.10 min	6.615	^{214}Pb
^{214}Pb	β^-	26.8 min	1.024	^{214}Bi
^{214}Bi	β^-	19.9 min	3.272	^{214}Po
^{214}Po	α	0.1643 ms	7.883	^{210}Pb
^{210}Pb	α	22.3 a	0.064	^{210}Bi

Table 4.2: Part of the radium series (source: [Fir99]).

4.3 Branching ratios for ^{214}Pb and ^{214}Bi gamma emissions

Gamma branching ratio for ^{214}Pb

Energy [keV]	Branching Ratio [%]
53.2275	1.2
241.997	7.43
295.224	19.3
351.932	37.6
785.96	1.07

Table 4.3: Main decay channels for ^{214}Pb gamma emissions (source: [Fir99])

Gamma branching ratio for ^{214}Bi

Energy [keV]	Branching Ratio [%]
609.3	46.1
665.453	1.46
768.356	4.94
806.174	1.22
934.061	3.03
1120.287	15.1
1155.19	1.63
1238.11	5.79
1280.96	1.43
1376.697	4.00
1401.5	1.27
1407.98	2.15
1509.228	2.11
1661.28	1.15
1729.595	2.92
1764.494	15.4
1847.42	2.11
2118.55	1.14
2204.21	5.08
2447.86	1.57

Table 4.4: Main decay channels for ^{214}Bi gamma emissions (source: [Fir99]

Bibliography

[BL98] V. Blobel and E. Lohmann, editors, *Statistische und numerische Methoden der Datenanalyse*, chapter Schaetzung von Parametern, Teubner Studienbuecher, 1998.

[Cle83] B. Cleveland, *The analysis of radioactive decay with a small number of counts by the method of maximum likelihood*, Nuclear Instruments and Methods **214**, 451–458 (1983).

[DLR11] Schlager and others. (DLR Collaboration), Probing the aged plume of the 2011 Fukushima nuclear power plant explosions: Aircraft borne pollutants measurements in the upper troposphere over Europe , unpublished, July 2011.

[Fir99] Firestone R.B. and Ekstroem L.P., *Periodic chart of the nuclides*, `http://nucleardata.nuclear.lu.se/NuclearData/toi/`, February 1999.

[Heu94] G. Heusser, Characteristics of the Gallex Spectrometer, in *Proceedings of the Second International Conference on TRENDS IN ASTROPARTICLE PHYSICS*, edited by P. Bosetti, B.G. Teubner Verlagsgesellschaft, 1994.

[Jam98] F. James, *MINUIT - Function Minimization and Error Analysis*, 94.1 edition, 1994-1998.

[Kae03] F. Kaether, Eichung der absoluten Nachweiswahrscheinlichkeiten von Zaehlrohren des Sonnenneutrino-Experiments GNO, Master's thesis, Ruprecht-Karls-Universitaet Heidelberg, 2003.

[Kae07] F. Kaether, *Datenanalyse des Sonnenneutrinoexperiments GALLEX*, PhD thesis, Ruprecht-Karls-Universitaet Heidelberg, 2007.

[Kay95] Kaye and Laby, *Tables of Physical and Chemical Constants*, `http://www.kayelaby.npl.co.uk/atomic_and_nuclear_physics/4_7/4_7_1.html`, 1995.

[Kih07] T. Kihm, *MIZZI Utilities/Libraries*, 3.2 edition, March 2007.

[Leo78] W. R. Leo, *Techniques for Nuclear and Particle Physics Experiments*, Springer-Verlag, 1978.

[Lin09] S. Lindemann, Reinigung und Nachweis von Edelgasen mit miniaturisierten Proportionalzaehlrohren, Master's thesis, Ruprecht-Karls-Universitaet Heidelberg, 2009.

[NIS09] NIST (National Institute of Standards and Technology), *ESTAR – stopping-power and range tables for electrons*, http://physics.nist.gov/PhysRefData/Star/Text/ESTAR.html, 2009.

[Sim03] H. Simgen, *Hochempfindlicher Nachweis radioaktiver Edelgasnuklide und natuerlicher Radionuklide aus der Uran-Zerfallsreihe*, PhD thesis, Ruprecht-Karls-Universitaet Heidelberg, 2003.

[SIS04] SIS GmbH, *SIS3000/SIS3001 65/80/100 MHz VME FADCs User Manual*, 3.40 edition, August 2004.

[Urb89] A. Urban, *Analyse von Proportionalzaehlrohrimpulsen zum Nachweis von solaren Neutrinos*, PhD thesis, Technische Universitaet Muenchen, 1989.

[Wal11] Wales J. and Sanger L., *Wikipedia*, http://en.wikipedia.org/wiki/Fukushima_Daiichi_nuclear_disaster#Explosion, July 2011.

Erklärung

Ich versichere, dass ich diese Arbeit selbständig verfasst und keine anderen als die angegebenen Quellen und Hilfsmittel benutzt habe.

Heidelberg, den 25.07.2011

Ludwig Rauch